Interplay between the Charge Transport Phenomena and the Charge-Transfer Phase Transition in $Rb_xMn[Fe(CN)_6]_y \cdot zH_2O$

Gábor Molnár,*,† Saioa Cobo,† Tarik Mahfoud,† Esther J. M. Vertelman,‡ Petra J. van Koningsbruggen,‡ Philippe Demont,*,§ and Azzedine Bousseksou*,†

Laboratoire de Chimie de Coordination, CNRS UPR-8241, Toulouse, France, Stratingh Institute for Chemistry, University of Groningen, Nijenborgh 4, 9747 AG Groningen, The Netherlands, Laboratoire de Physique de Polymères, CIRIMAT, CNRS UMR-5085, Université Toulouse III, Toulouse, France

Charge transport and dielectric measurements were carried out on compacted powder and single-crystal samples of bistable $Rb_xMn[Fe(CN)_6]_y \cdot zH_2O$ in the two valence-tautomeric forms ($Mn^{II}Fe^{III}$ and $Mn^{III}Fe^{II}$) as a function of temperature (120–350 K) and frequency ($10^{-2}–10^6$ Hz). The complex conductivity data reveal universal conductivity behavior and obey the Barton–Nakajima–Namikawa relationship. The charge transport is accompanied by dielectric relaxation that displays the same thermal activation energy as the conductivity. Surprisingly, the activation energy of the conductivity was found very similar in the two valence-tautomeric forms (~0.55 eV), and the conductivity change between the two phases is governed mainly by the variation of the preexponential factor in each sample. The phase transition is accompanied by a large thermal hysteresis of the conductivity and the dielectric constant. In the hysteresis region, however, a crossover occurs in the charge transport mechanism at $T < \sim220$ K from an Arrhenius-type to a varying activation energy behavior, conferring an unusual "double-loop" shape to the hysteresis.

1. Introduction

The mixed-valence compound $KFe[Fe(CN)_6]$ (Prussian blue) and related cyanide complexes of transition metal ions have been extensively investigated in the past because of their interesting electronic structure[1] as well as for their appealing optical properties[2] and rich electrochemistry.[3] More recently, they have received much attention also for their remarkable magnetic properties, such as high Curie temperatures[4] and photomagnetism.[5] In some of these complexes, a charge transfer phase transition, associated with a metal-to-metal electron transfer, occurs due to the strong electron–lattice interactions. For example, the compound $Na_xCo[Fe(CN)_6]_y \cdot zH_2O$ exhibits (in certain x, y, z stoichiometries) a first-order thermal phase transition between the $Fe^{III}(S = 1/2)–CN–Co^{II}(S = 3/2)$ and the $Fe^{II}(S = 0)–CN–Co^{III}(S = 0)$ states.[6] These two phases display markedly different magnetic, optical, and electrical properties. Concerning this latter property, Sato et al.[7] reported recently that the conductivity-vs-temperature curve in this compound displays a hysteresis loop similar to that observed in the variable temperature magnetic susceptibility measurements.

A few investigations have already considered the electrical conductivity of Prussian blue and its analogues in the solid state.[8–11] Similar to other low-mobility, disordered solids, the charge transport is thought to take place in these materials due to hopping conduction. In general, a nearest-neighbor electron transfer is considered as the predominant process, but ionic conductivity may also occur to some extent, especially in wet samples. In this latter case, apparently, alkali metal ions are transported in their hydrated forms, and the water molecules present in the interstices lower significantly the barriers to the

movement of these ions. In any case, the charge transport is accompanied by dipole relaxation phenomena. In samples with low water content, the dipole motion corresponds to the intervalence charge transfer between the two transition metal sites ($M_A^{2+}–CN–M_B^{3+} \leftrightarrow M_A^{3+}–CN–M_B^{2+}$). By determining the rate at which these dipole moments are oscillating, one can thus determine the rate of the intervalence electron transfer. Unfortunately, the comparison of data obtained on different samples is not straightforward, owing to their nonstoichiometric, disordered nature and the presence of water in the interstices of the lattice, which are difficult to control in the experiments. For this reason, the possibility to investigate the same sample under the same conditions (T, P, etc.) but in two different electronic states (coexisting within a large thermal hysteresis region) offers a unique opportunity to investigate the mechanism of the charge transport in this family of compounds and, in particular, the influence of the electronic and crystallographic structure on the site-to-site electron hopping process and associated dipole relaxation phenomena. In addition to these fundamental aspects, it is also of interest to see if the conductivity changes accompanying the phase transition in this type of compounds can be sufficiently important to be eventually used in practical applications, such as memory or switching devices.

In this paper, we report on the charge transport and dielectric properties of the bistable Prussian blue analogue $Rb_xMn[Fe(CN)_6]_y \cdot zH_2O$ investigated in a broad frequency range ($10^{-2}–10^6$ Hz). We have chosen this compound[12–14] because it presents an exceptionally large thermal hysteresis loop (up to 138 K),[15] thus providing a large range of temperatures for electrical measurements in the two phases. The high-temperature (HT) $Fe^{III}(S = 1/2)–CN–Mn^{II}(S = 5/2)$ form of this compound has a face-centered cubic structure ($F\bar{4}3m$), whereas in the low-temperature (LT) $Fe^{II}(S = 0)–CN–Mn^{III}(S = 2)$ phase, the crystal structure is tetragonal ($I\bar{4}m2$) and the MnN_6 octahedra

* Corresponding authors. E-mails: (G.M.) molnar@lcc-toulouse.fr, (A.B.) boussek@lcc-toulouse.fr, (P.D) demont@cict.fr.
† Laboratoire de Chimie de Coordination, CNRS, Toulouse.
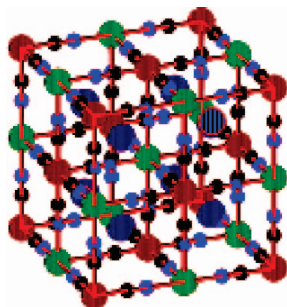‡ University of Groningen.
§ Université Toulouse III.

Charge Transport, Transfer in Rb$_x$Mn[Fe(CN)$_6$]$_y$·zH$_2$O

J. Phys. Chem. C, Vol. 113, No. 6, 2009 **2587**

Figure 1. Representation of the unit cell of RbMn[Fe(CN)$_6$]·H$_2$O.[20]

Figure 2. Temperature dependences of the dc conductivity (measured at 2 and 20 V bias) and the effective magnetic moment for sample **1**.

show a Jahn−Teller-type distortion.[16] It should be noted, however, that for low Rb$^+$ content, the LT phase was reported to retain the cubic structure. In any case, the formation of the LT phase is accompanied by a discontinuous lattice contraction of ∼10% and a reduction of the average Fe−Mn distance from 5.27 to 5.10 Å.[17] It is important to note also that the width and the position of the hysteresis loop in this compound depends strongly on the particular *x*, *y*, *z* stoichiometry obtained during the precipitation of the compound, since the extreme insolubility makes for difficulty in achieving exactly reproduced compositions.[18,19] For stoichiometries close to the idealized *x* = *y* = 1 composition, the phase transition occurs around 230 and 300 K in the heating and cooling cycles, respectively. In most cases, however, the system contains [Fe(CN)$_6$]$^{3-}$ vacancies (Figure 1). The formation of these vacancies leads to lower Rb$^+$ concentration (*x*) to maintain the charge neutrality. Moreover, the H$_2$O content (*z*) increases, since the water molecules complete the coordination around the Mn^{II} ion at the place of the missing [Fe(CN)$_6$]$^{3-}$ ligands. This change in the coordination sphere of the Mn^{II} ions leads to a significant lowering of the ligand field and stabilization of the HT phase; hence, the transition temperature decreases, and the hysteresis loop becomes larger.[18] If the vacancy concentration exceeds a certain limit (*y* < ∼0.9), the compound remains in the HT state down to liquid helium temperatures.[19]

2. Experimental Section

Four polycrystalline samples of Rb$_x$Mn[Fe(CN)$_6$]$_y$·zH$_2$O with different stoichiometries have been synthesized following "method 2" described in ref 19. The precipitates were filtered, washed with water, dried at 90 °C, and kept in a desiccator at room temperature between the different measurements. The composition of the obtained brown powders was established from elemental analysis as Rb$_{0.76}$Mn[Fe(CN)$_6$]$_{0.91}$·1.6H$_2$O (**1**), Rb$_{0.82}$Mn[Fe(CN)$_6$]$_{0.96}$·0.7H$_2$O (**2**), Rb$_{0.96}$Mn[Fe(CN)$_6$]$_{0.98}$·0.75H$_2$O (**3**), and Rb$_{0.38}$Mn[Fe(CN)$_6$]$_{0.82}$·4.5H$_2$O (**4**). Single crystals of RbMn[Fe(CN)$_6$]·H$_2$O (**5**) were grown by the method described in ref 20.

The dc and ac conductivity measurements have been carried out in the two-probe geometry either on powder samples (diameter 10 mm, thickness ∼0.1 mm) contained in a Teflon sample holder between two stainless steel electrodes or on pellets (diameter 3.3 mm, thickness 0.4 mm) compacted at a pressure of 70 bar for 5 min. There were no significant differences in conductivities or magnetic susceptibilities between the powder samples and pellets, although the latter gave, in general, somewhat better results in terms of standard deviation of the measured conductivity values. In the case of single crystals (∼1 mm size), electrical contacts were fixed using a silver paste. Direct current as a function of applied dc voltage (0.05−20 V) and temperature (160−350 K) were measured using a Keithley
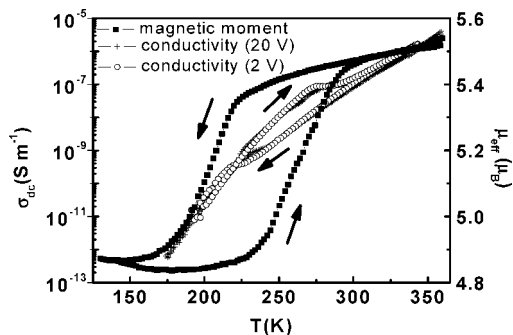
Instruments Inc. (Cleveland, OH) model 617 electrometer and a home-built, electrically shielded, He-exchange gas cryostat. The temperature was varied at a rate of 1 K min^{-1}. AC conductivity measurements were carried out as a function of frequency (10^{-2}−10^6 Hz) and temperature (120−350 K) by means of a BDS4000 broadband dielectric spectrometer coupled to a Quatro Cryosystem (Novocontrol Technologies, Hundsangen, Germany) at an applied ac voltage of 1 V. Frequency sweeps were carried out isothermally. Thermoelectric power *S* (= d*V*/ d*T*) measurements were performed on pellets using a device described elsewhere.[21] The Seebeck coefficients could be determined only above ∼300 K because of the high resistance of the samples at lower temperatures. Variable-temperature dc magnetic susceptibility measurements were carried out on powder, pellet, and single-crystal samples at heating and cooling rates of 1 K min^{-1} using a Quantum Design (San Diego, CA) MPMS2 SQUID magnetometer operated at 2 T magnetic field. The magnetic properties of the samples were checked several times during the experiments, and no significant evolution has been observed.

3. Results

Figure 2 shows the temperature dependence of the effective magnetic moment (μ_{eff}) for compound **1**. The μ_{eff} value at 300 K (HT phase) is 5.5 μ_B. When decreasing the temperature, μ_{eff} decreases slowly and drops more abruptly between ∼210 and 190 K. At 150 K, it reaches the value of 4.9 μ_B. When heating the sample, the reverse transition occurs in the 235−295 K temperature range. It should be noted that the HT value of the magnetic moment differs significantly from the expected spin-only value of 6.1 μ_B. Such differences have been observed previously[19] and can be attributed to the incomplete nature of the phase transition. The temperature dependence of the dc conductivity, σ_{dc}, (measured at 2 and 20 V) is shown in Figure 2, together with the magnetic data. At 300 K, the electrical conductivity is ∼10^{-7} S m^{-1}, which is 2 orders of magnitude higher than that reported for vacuum-dried Prussian blue.[8] σ_{dc} is strongly thermally activated in the investigated temperature range and drops to 10^{-12} S m^{-1} at 180 K. The conductivity displays a large thermal hysteresis loop between ∼220 and 300 K. The hysteresis region on the high temperature side corresponds well to the magnetic data, but a significant difference is observed on the low temperature side. Between 210 and 170 K, where the HT phase transforms to the LT phase, the conductivity has a similar value independently if it is recorded in the heating or cooling cycles. In a first instance, one may suppose therefore that there is a crossover in the conduction mechanism around 220 K and the conductivity becomes rather
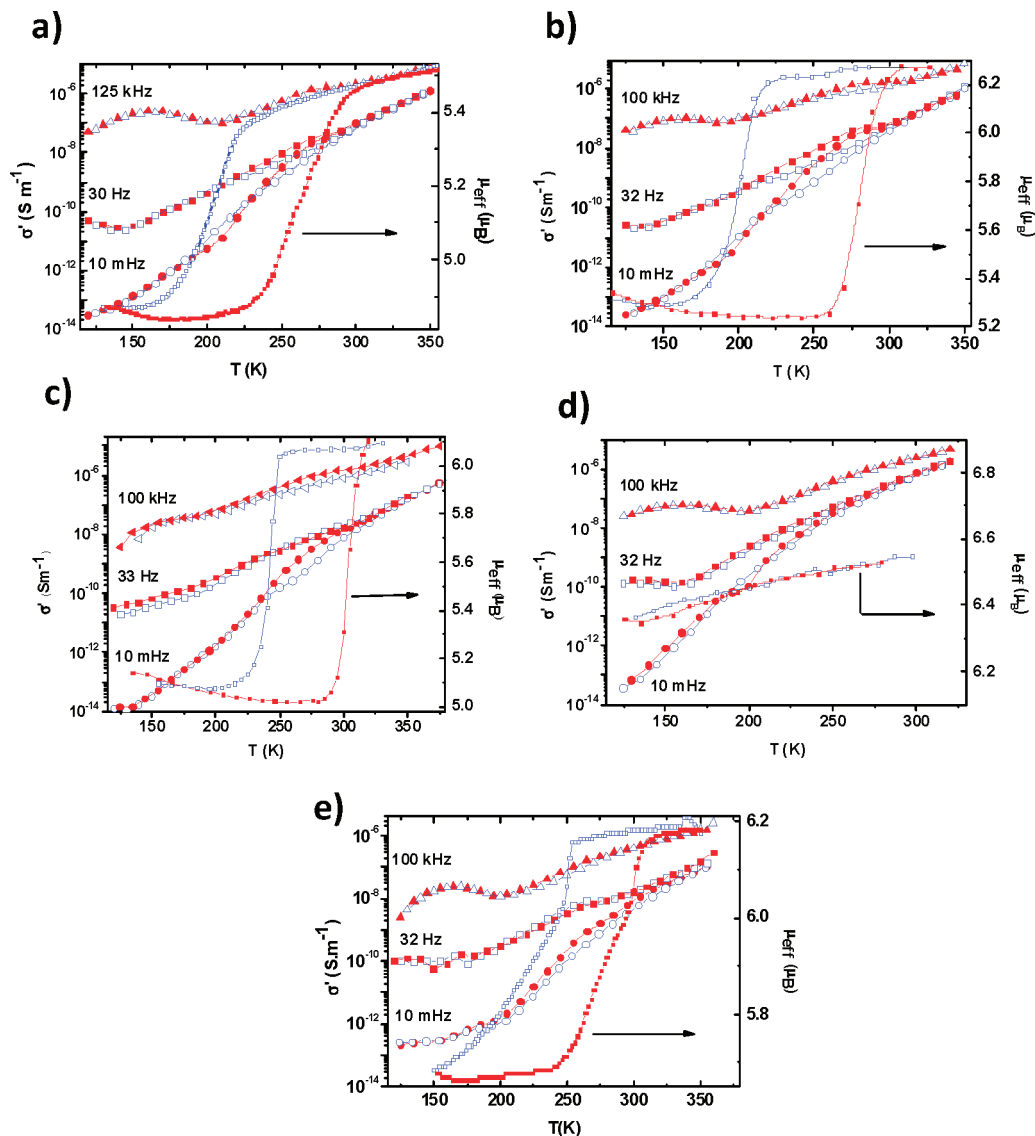
Figure 3. Temperature dependence of the ac conductivity at different frequencies and the effective magnetic moment for samples **1** (a), **2** (b), **3** (c), **4** (d) and **5** (e). Closed and open symbols correspond to the heating and cooling cycles, respectively. Data points are connected to guide the eye.

insensitive to the actual electronic and crystallographic form below the crossover point.

Current-vs-electric-field (corresponding to an applied dc voltage bias between 50 mV and 20 V) data were also recorded at different temperatures. The same currents were measured for a given field independently if it was reached by increasing or decreasing the applied voltage. A slight deviation from the ohmic behavior appeared, but no significant difference in the electric field dependence could be observed below, around, and above the crossover point at 220 K.

To better understand the possible origin of this crossover point and the effects of the valence-tautomeric phase transition, we have investigated the frequency as well as temperature-dependent behavior of the complex conductance. The temperature dependence of the real part $\sigma'(\omega)$ of the ac conductivity is shown in Figure 3 for the different samples. In sample **1**, at 125 kHz, the conductivity exhibits very weak temperature dependence, and no hysteresis is observed (Figure 3a). At 10 mHz, the temperature dependence of the ac conductivity is the same, within the measurement errors, as that of σ_{dc} (σ' (300 K) = 9.6 $\times$ 10^{-8} S m^{-1} and σ' (180 K) = 1.3 $\times$ 10^{-12} S m^{-1}). At this frequency, σ' exhibits a hysteresis, which corresponds well to

the hysteresis region detected by magnetic measurements, but a crossing of the heating and cooling curves occurs in the hysteresis region around 230 K, very close to the crossing observed in the dc measurement. The conductivity behavior at 30 Hz appears to be intermediate between the high- and low-frequency cases. Samples **2** and **3** exhibit somewhat different phase transition temperatures, and thus, the thermal hysteresis of the magnetic moment differs to some extent. For sample **2**, we observed σ' (300 K, 10 mHz) = 5 $\times$ 10^{-8} S m^{-1} and σ' (180 K, 10 mHz) = 1.2 $\times$ 10^{-12} S m^{-1} and a conductivity hysteresis loop between 170 and 305 K with a crossover point close to 220 K (Figure 3b). In the case of sample **3**, the measured values (σ' (300 K, 10 mHz) = 1.6 $\times$ 10^{-8} S m^{-1} and σ' (180 K, 10 mHz) = 4.2 $\times$ 10^{-13} S m^{-1}) are close to those of the two other compounds. On the other hand, in this sample, the phase transition is practically complete at 220 K, which explains why one cannot observe the crossover in the conductivity hysteresis (Figure 3c). Similar results were obtained on the single-crystal sample **5**, as well (Figure 3e), but the ill-defined electrode geometry makes the data analysis more difficult (vide infra). We have also measured the ac conductivity in sample **4**, which does not exhibit charge transfer phase transition and remains
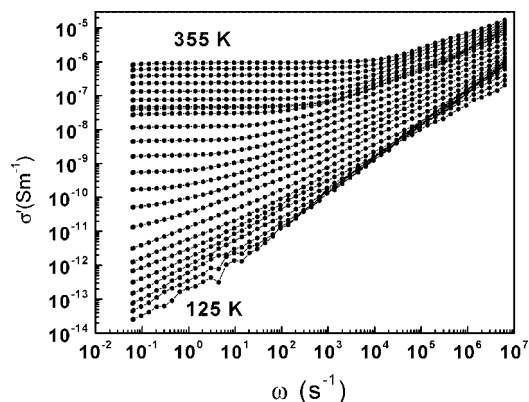
Figure 4. Frequency dependence of the ac conductivity for sample **2** at fixed temperatures in the heating cycle. Curves are displayed by steps of 10 K. Data points are connected to guide the eye.

Figure 5. Temperature dependence of the dielectric constant (ε') at 2 kHz for samples **1**−**4**. Closed and open symbols correspond to the heating and cooling cycles, respectively. Data points are connected to guide the eye.

in the HT phase in the whole temperature range. The conductivity of this sample was found somewhat higher than the two others (σ' (300 K, 10 mHz) = 7.0×10^{-7} S m^{-1} and σ' (180 K, 10 mHz) = 3.2×10^{-11} S m^{-1}), and no hysteresis of σ occurs (Figure 3d).

The temperature dependence of the ac conductivity can be better understood from Figure 4, which displays the frequency dependence of σ' at different temperatures for sample **2** in the heating mode. (Analogous behaviors were observed on heating and cooling in each sample, which are, therefore, omitted.) At high temperatures and low frequencies, σ' is constant and closely matches the dc values. As the frequency increases, a gradual dispersion sets in, resulting in an apparent power law dependence ($\sigma' \sim \omega^n$) with an exponent $n \cong 0.6$ at high temperatures. The crossover frequency (ω_c) that separates the power-law and the frequency-independent (dc) regimes decreases continuously with decreasing temperature from ~0.5 kHz to 10 mHz between 345 and 225 K. This behavior is typical to disordered solids consisting of regions with different conductivities.[22] At high frequencies, the carrier motion is localized, but as the frequency decreases, charge transport must extend over longer distances and will be increasingly limited by bottlenecks of poorly conducting regions; therefore, the conductivity decreases, as well. The fact that the temperature dependence of σ' in the power-law regime is less pronounced is consistent with the observation that the thermal hysteresis becomes less detectable at high frequencies and low temperatures.

The measurement of the impedance allows one to determine both the complex conductivity and the complex dielectric function, which are related to each other by $\sigma^* = i\omega\varepsilon_0\varepsilon^*$ (ε_0 being the permittivity of the free space). The motion of the charge carriers in low-mobility solids is accompanied by an electrical relaxation; therefore, the analysis of ε' (or σ'') can contribute to the understanding of the charge transport mechanisms. In Prussian blue analogues, the electron transfer between the metallic sites is accompanied by a change in the direction of the dipole moments in the sample (for example, $Mn^{II} \rightarrow Fe^{III}$ vs $Mn^{III} \leftarrow Fe^{II}$). Therefore, one can expect a significant difference in ε' with the phase transition between the HT and LT forms of $Rb_xMn[Fe(CN)_6]_y \cdot zH_2O$. Ohkoshi et al.[23] recently reported dielectric constant measurements on this compound both in the radio frequency (1−100 kHz) and optical (300−1000 THz) regions. Though reflecting different processes (dipolar and electronic) ε' was found to change significantly upon the phase transition in both frequency domains and the observed hysteresis loop was comparable with the magnetic susceptibility data. In our case, we investigated ε' in the 10 mHz−1 MHz frequency
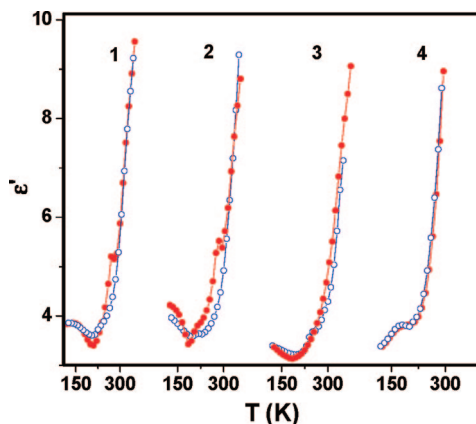
domain. As an example, Figure 5 shows the thermal variations of ε' measured at 2 kHz for the different samples (with and without thermal hysteresis of the magnetic moment). The main observation here is that the temperature dependence of the dielectric constant corresponds also to the hysteresis of the magnetic moment. As in the conductivity data, a crossing of cooling and heating curves appears in the hysteresis region close to 220 K. In the low temperature limit, ε' has a value close to 3.5−4 in each sample, similar to what was reported by Ohkoshi et al.[23]

Unfortunately, the frequency and temperature dependences of the dielectric permittivity are difficult to analyze by means of the conventional Cole−Cole representation because a strong low-frequency dispersion of ε' and ε'' appears when the temperature increases. This behavior is characteristic of charged carrier systems.[24] By using the electric modulus formalism for the treatment of dielectric data, an enhancement of the contribution of conductivity effects can be obtained.[25] The conductivity relaxation model, in which a dielectric modulus is defined by $M^*(\omega) = 1/\epsilon^*(\omega)$, can be used to obtain information about the relaxation mechanism in the absence of a well-defined dielectric loss peak. As far as conductive effects are concerned, the electric loss moduli $M''(\omega)$ exhibit relaxation maxima, in contrast to the relatively smooth patterns of $\varepsilon''(\omega)$ plots. Another advantage arises from the fact that the contribution of the electrode screening effect in the low-frequency spectrum tail can be eliminated. To estimate the dielectric relaxation in $Rb_xMn[Fe(CN)_6]_y \cdot zH_2O$ samples, the complex permittivity is converted to the complex electric modulus. As an example, Figure 6 displays the imaginary part of the electric modulus (scaled by M''_{max}) as a function of the frequency of the electrical field (scaled by ω_{max}) at different temperatures in the heating cycle for sample **2**. (Analogous behaviors were observed on heating and cooling in each sample, which are, therefore, omitted. The perfect overlap of the curves for the investigated temperatures leads to a master curve. This means that all dynamic processes occurring at different temperatures exhibit a similar activation energy and that the distribution of the relaxation time is independent of temperature. The frequency of the M'' peak maximum is defined as the dielectric relaxation frequency (ω_p), and it was found to increase with increasing temperature.

4. Discussion

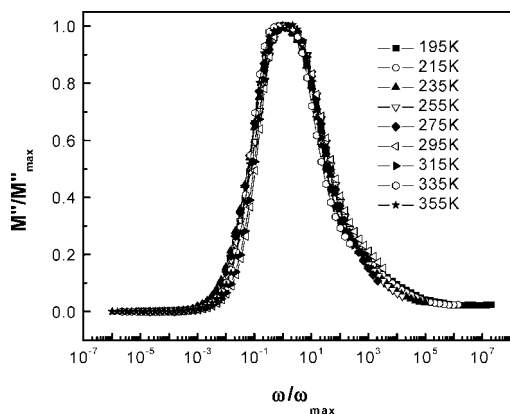**Charge Transport and Dielectric Relaxation.** The temperature dependence of the dc conductivity of each Rb_xMn-

Figure 6. Plot of normalized loss electric modulus (M''/M''_{max}) vs reduced frequency (ω/ω_{max}) at various temperatures in the heating cycle for sample **2**. Curves are displayed by steps of 20 K. Data points are connected to guide the eye.

$[Fe(CN)_6]_y \cdot zH_2O$ sample exhibits two regions, independent of if they exhibit charge transfer phase transition. Above ~220 K, the temperature dependence of the dc conductivity is described, as expected for a small polaron hopping mechanism, by an Arrhenius equation:[26]

$$\sigma_{dc}(T) = (B/T) \exp(-E_{dc}/k_B T) \qquad (1)$$

The activation energy of the dc conductivity (E_{dc}) was 0.57 (1), 0.56 (2), 0.51 (1), and 0.43 (1) eV for samples **1**, **2**, **3** and **4**, respectively (Table 1). The activation energies were found to be the same within the experimental uncertainty in the HT and LT phases. (We shall note here that the E_{dc} values have been extracted actually from the frequency-independent part of the ac conductivity data, displayed in Figure 3.) One may speculate that the smaller activation energy obtained in the case of sample **4** is due to its significantly higher water content and associated higher dielectric constant.[8] When the temperature decreases below ~220 K, deviations from eq 1 indicate the presence of a change in the conduction mechanism. In fact, the observation of a variable activation energy (i.e., non-Arrhenius) conduction mechanism at low temperatures is a quite general feature of small polaron hopping.[27] As has been discussed by Austin and Mott, at relatively low temperatures, the zero-point energy allows polaron hopping to occur without any thermal activation.[28] These authors predicted a departure from the linear $\ln(\sigma_{dc}T)$ vs T^{-1} behavior for temperatures below $T = \theta_D/2$, where θ_D is defined by

$$k_B\theta_D = \hbar\omega_{ph} \qquad (2)$$

with ω_{ph} being the average (or predominant) phonon frequency. In our case, this phonon frequency ω_{ph} can be calculated as 5.8×10^{13} s^{-1} (~310 cm^{-1}), which falls in the range of typical frequencies of breathing modes of the metal-coordination polyhedra in Prussian blue analogues.[29]

As mentioned before, the conduction due to a process of site-to-site charge transfer must involve a dielectric relaxation. This is because a hop to a new site can lead to successful charge transport only if the polarization cloud follows. This electric relaxation requires a relaxation time, τ. With increasing frequency, the polarization (or dielectric constant) will monotonically decrease because the relaxation cannot follow the electrical field beyond a certain frequency. Indeed, this has been observed in our samples, as well. On the low frequency side, the dispersion of ε' has its physical origin in electrode polarization effects. On the other hand, at higher frequencies,

the analysis of the electrical modulus reveals a dipole relaxation process, which is thermally activated. To determine with more precision the frequency of the dielectric relaxation peaks, the experimental data of the dielectric loss modulus $M''(\omega)$ can be conveniently fitted by a superposition of two or three Havriliak−Negami functions,[30]

$$M''(\omega) = \sum_{j=1} \frac{\Delta M_j}{[1 + (i\omega\tau_j^{HN})^{\alpha_j}]^{\beta_j}} \qquad (3)$$

where $\tau^{HN} = 1/\omega_p[\sin \alpha\pi/2(1 + \beta)]^{1/\alpha}[\sin \alpha\beta/2(1 + \beta)]^{-1/\alpha}$ and ΔM are the mean relaxation time of the relaxation time distribution and the relaxation strength, respectively. The two shape parameters α and β determine the logarithmic slope of the low-frequency loss tail α and the high-frequency loss tail $-(\alpha\beta)$. In both samples, ω_p exhibits a thermally activated dependence; that is, it obeys the Arrhenius equation:

$$\omega_p(T) = \omega_{0p} \exp(-E_p/k_B T) \qquad (4)$$

Figure 7 shows the Arrhenius plot of the two main relaxation frequencies for sample **2** (in the heating cycle). The two main relaxation processes show very similar temperature dependences, although the values of the preexponential factor ω_{0p} are somewhat different. Figure 7 also displays the temperature dependence of the crossover frequency, ω_c, determined from the ac conductivity data of the same sample. Indeed, the frequency dependence of σ' is usually well-described by using Jonscher's "universal dielectric response" (UDR),[24]

$$\sigma'(\omega) = \sigma_{dc} + A\omega^n = \sigma_{dc}[1 + (\omega/\omega_c)^n] \qquad (5)$$

where the characteristic frequency, ω_c, corresponds to the onset of the conductivity dispersion and n is the frequency exponent, which has a value around 0.6 ($\pm$ 0.05) in the high temperature range (see the inset of Figure 7). The crossover frequency corresponds to the hopping frequency, ω_h, of the charge carriers and shows a thermal variation similar to the dielectric modulus loss peak maximum. Indeed, as seen in Figure 7, the hopping frequency is also thermally activated for sample **2**, and it is fitted to the Arrhenius equation,

$$\omega_h(T) = \omega_{0h} \exp(-E_h/k_B T) \qquad (6)$$

where E_h is the activation energy for hopping and ω_{0h} is the attempt frequency. Upon comparing the values of E_p (0.55(1) eV) and the activation energy of hopping (E_h = 0.53(2) eV) in the LT phase (heating mode), it can be assumed that these two representations are completely equivalent, even if they emphasize different aspects of the underlying mechanisms of charge transport.

In Figure 8, the temperature dependence of direct current conductivity, using eq 1, is compared to the temperature behavior of the main relaxation frequency ω_p (see eq 4) for sample **2**. Table 1 summarizes the fitting results for each sample. The activation energy of the relaxation frequency (E_p) was evaluated as ~0.54(1), 0.56(1), and 0.42(2) eV for samples **2**, **3**, and **4**. The fact that $E_{dc} \cong E_p$ implies that the charge carrier has to overcome the same energy barrier while conducting as well as relaxing. The observed dielectric relaxation is therefore due to the electrical conduction. This also means that ω_p and σ_{dc} are proportional and the constant of proportionality is universal, varying only weakly with the temperature. This finding is known as the Barton−Nakajima−Namikawa relationship and indicates that the dc and ac conductivities are closely related to each other and based on the same mechanism of charge transport. Indeed, the frequency-dependent conductivity

Charge Transport, Transfer in Rb$_x$Mn[Fe(CN)$_6$]$_y$·zH$_2$O

J. Phys. Chem. C, Vol. 113, No. 6, 2009 **2591**

TABLE 1: DC Conductivity and Dielectric Relaxation Activation Parameters for the Different Samples of Rb$_x$Mn[Fe(CN)$_6$]$_y$·zH$_2$O in the LT and HT Phases Derived Using Eqs 1 and 4, Respectively

	LT		HT		LT		HT	
	E_{dc} (eV)	B (S cm^{-1} K)	E_{dc} (eV)	B (Scm^{-1}K)	E_p (eV)	ω_{0p} (s^{-1})	E_p (eV)	ω_{0p} (s^{-1})
1	0.57 ± 0.01	9200 ± 300	0.57 ± 0.01	1120 ± 110	a	a	a	a
2	0.54 ± 0.01	670 ± 130	0.57 ± 0.01	450 ± 130	0.55 ± 0.01	$(3.2 \pm 1.6) \times 10^{13}$	0.53 ± 0.01	$(1.4 \pm 0.6) \times 10^{12}$
3	0.50 ± 0.01	820 ± 130	0.51 ± 0.01	770 ± 160	0.56 ± 0.01	$(8.0 \pm 1.6) \times 10^{12}$	0.57 ± 0.01	$(1.9 \pm 1.9) \times 10^{12}$
4	no phase transition		0.44 ± 0.01	45 ± 4	no phase transition		0.42 ± 0.02	$(4.8 \pm 0.2) \times 10^{11}$
5	a	a	0.52 ± 0.01	810 ± 80	a	a	0.50 ± 0.01	$(9 \pm 3) \times 10^{9}$

a No reliable data.

of many disordered materials (inorganic glasses, polymers, doped semiconductors, and ionic conductors) is known to exhibit such universality, and their behavior can be scaled to a master curve (i.e., the conductivity data follow the time−temperature superposition).[24]

The above discussion was restricted to compacted powder samples because they provided the highest quality complex conductivity data (due to their favorable electrode geometry). However, in polycrystalline materials, in addition to bulk conductivity, grain boundary resistance, and polarization have to be considered, as well, especially in the low-frequency range. Under the action of an electric field, the grains are polarized by the accumulation of charge carriers on their boundaries, leading to an additional relaxation component in the dielectric spectrum of the material. In many cases, separation of the bulk and grain boundary effects is straightforward by means of Cole−Cole type plots of the complex impedance (or permittivity) data. In our case, Cole−Cole arcs did not apply and only a continuous increase of ε'' with ε' was observed. For this reason, we used the modulus formalism for separating interfacial phenomena from dipole relaxation due to charge hopping. For further investigation of eventual grain boundary effects on the complex conductivity of this material, we have investigated a single crystal sample of RbMn[Fe(CN)$_6$]·H$_2$O, as well (sample **5**).[20] Due to the small size (∼1 mm^3) and nongeometrical shape of the available crystals, the electrode geometry is ill-determined, and this leads to high uncertainty in the absolute value of the conductivity and also to a higher standard deviation of the data, especially at low temperatures. Nevertheless, the conductivity data on single crystals closely resembles those obtained on polycrystalline samples (Figure 3e). Notably, we noticed a marked deviation from an Arrhenius-type behavior below 220 K. Between 350 and 220 K, the conductivity falls 4 orders of magnitude, similar to the polycrystalline case, which corresponds

to a thermal activation energy of ∼0.52 eV (Table 1). Note here that in the single crystals, the phase transition takes place rather gradualy between the pure HT phase and a mixed (1:1) HT + LT form, and therefore, fitting cannot be carried out in the LT phase. However, it appears clearly that both the relaxation frequency and the conductivity of the LT form are higher when compared to the pure HT phase (at a given temperature). The frequency dependence of the conductivity follows a power law, and as a consequence, the hysteresis of the conductivity disappears at higher frequencies. The electric loss moduli $M''(\omega)$ exhibit temperature-dependent relaxation maxima, and the $M'(\omega)$ curves at different temperatures can be scaled to a master curve similar to the powder samples. The activation energy of the relaxation is ∼0.50 eV. This means that in the crystals, as well, the relationship $E_{dc} \cong E_p$ is confirmed. The main difference between the single crystal and polycrystalline samples is observed below ∼200 K in the low-frequency region, where the crystals show significantly less temperature-dependent (virtually activationless) conductivity. Since there is no single straightforward theory that may allow us to discuss the mechanism of this low-temperature conductivity process and the quality of the data is also rather poor at low temperatures, the discussion of the interplay between the charge transport and the charge-transfer phase transition will be confined to the high-temperature region (>220 K).

Charge Transport and the Charge Transfer Phase Transition. As shown in Figures 2, 3, and 5, the thermal hysteresis of the magnetic susceptibility can be clearly correlated with a hysteresis of the dc conductivity as well as the dielectric permittivity. However, inside the hysteresis region, a crossing point appears in $\sigma_{dc}(T)$ as well as in $\varepsilon'(T)$ around 210−230 K, leading to a strange "double-loop" curve, which is not observed in the magnetic measurements. Clearly, this crossing point is not related to the charge-transfer phase transition, since it is observed in sample **4**, neither is it related to another structural
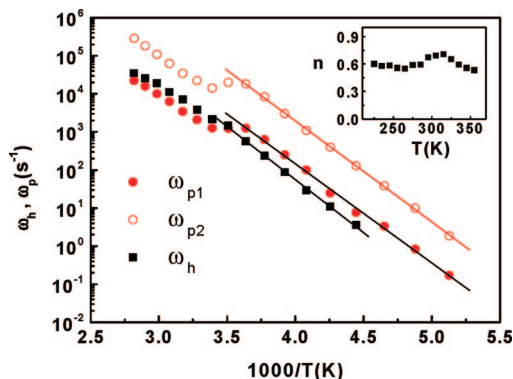

Figure 7. Arrhenius plot of the relaxation frequencies, ω_p, obtained from the maximum in $M''(\omega)$ and ω_h, obtained from the nonlinear least-squares fitting of $\sigma'(\omega)$ to eq 5 (sample **2**, heating cycle). The solid lines are the least-squares linear fits to eqs 4 and 6. The insert shows the thermal variation of the power exponent n in eq 5.
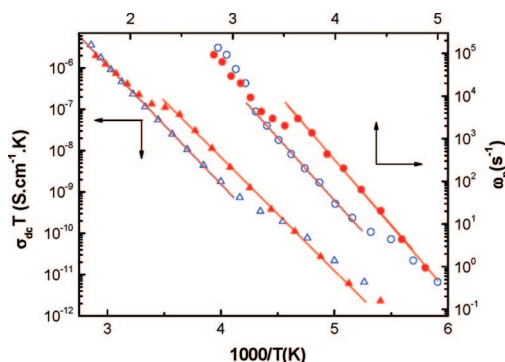

Figure 8. Temperature dependence of the dc conductivity (triangles) and the conductivity relaxation frequency (circles) for sample **2**. Closed and open symbols correspond to the heating and cooling cycles, respectively. The solid lines are the least-squares linear fits to eqs 1 and 4.

2592 *J. Phys. Chem. C, Vol. 113, No. 6, 2009*

Molnár et al.

modification, since powder X-ray diffraction, Raman spectroscopic, and differential scanning calorimetric measurements revealed no singularity around 220 K. Therefore, we believe that this crossing point is not related to any structural change in the sample and should be associated with a departure from an Arrhenius-like hopping process toward an activationless, tunneling conduction mechanism (as described above).

In the high-temperature range, our observations point clearly to a conduction mechanism by small polaron hopping. Given that the water content of our samples was kept as low as possible, we adopt the hypothesis of Rosseinsky et al.,[10] and we assign this hopping process to an intervalence electron transfer, $Mn^{2+}-NC-Fe^{3+} \leftrightarrow Mn^{3+}-NC-Fe^{2+}$. This assignment is corroborated by our thermopower measurements because the sign of the Seebeck coefficient was negative in each sample. (Typically, S exhibits values of about -120 (± 20) μV/K between 300 and 350 K.) Bearing in mind that this assignment concerns only the high-temperature region, the possible effects of the phase transition on the charge transport will now be considered. In the case of hopping transport, we can use the well-established relationship, using the Einstein diffusion equation, between the dc conductivity and the hopping frequency,[26]

$$\sigma_{dc} = (n_c e^2 a^2/6k_B T)\nu_p = (n_c e^2 a^2/6k_B T)\nu_{0p}[\exp(-E_p/k_B T)]$$
(7)

where $\nu_p = \omega_p/2\pi$, a is the hopping distance (i.e., the Fe–Mn distance), n_c is the carrier density (i.e., the density of Fe–Mn pairs), and E_p is the activation energy for the hopping process. This equation implies that the activation energy for ω_p and σ_{dc} is the same ($E_p = E_{dc}$), which we have already demonstrated above. A further proof for the applicability of eq 7 in the present case comes from the evaluation of n_c, which appears to be on the order of $3(\pm 2) \times 10^{26}$ m^{-3} and nearly independent of the temperature. This value is reasonably close to the theoretical number density of Fe–Mn pairs of 3.4×10^{27} m^{-3} in RbMn[Fe(CN)$_6$]·H$_2$O if one takes into account that the hopping probability will be necessarily reduced to some extent in the real material due to the vacant metallic sites, charge disorder, and interactions between the polarons.[27]

Figures 2 and 3 reveal clearly that the dc conductivity is higher in the LT phase. Let us note that the same observation was made by Sato et al. in the case of the compound Na$_x$Co[Fe(CN)$_6$]$_y$·zH$_2$O.[7] In the case of Rb$_x$Mn[Fe(CN)$_6$]$_y$·zH$_2$O, the higher conductance (σ_{dc}) of the LT phase parallels the higher hopping frequencies (ω_p) (Figure 8), which can be explained either by a lower activation barrier (E_p) or by a higher value of the preexponential factor (ω_0). In our samples **1** and **2**, the activation energy in the HT and LT phases was very similar (0.54 $\pm$ 0.03 eV) (Table 1), whereas in the sample investigated by Sato et al., the activation energy of the dc conductivity was even smaller in the HT phase (0.34 eV) when compared to the LT phase (0.54 eV). This points to the important role of the preexponential factor, which increases in the case of sample **2** (for example) from (1.5 $\pm$ 0.6) $\times 10^{12}$ s^{-1} to (3.8 $\pm$ 2.6) $\times 10^{13}$ s^{-1} when going from the HT to the LT phase. These values of ω_0 are of the order of the lattice phonon frequencies to which carriers can be coupled. This central role of the phonons would not be surprising, since strong electron–phonon interaction is a prerequisite for small polaron formation, and the charge transfer phase transition also involves a strong modification of the lattice dynamics. Indeed, the LT phase is much stiffer due to its reduced volume, and the Jahn–Teller distortion in the LT phase also alters the electron–phonon coupling scheme.

Even if the uncertainty of the absolute values of ω_0 are relatively high, we stress that we observed an increase in the preexponential factor upon the HT → LT transition for each sample, both in the dc conductivity and, independently, in the dielectric relaxation data while the activation energy remained close to constant. One should also note that the value of ω_0 cannot be directly associated with a particular phonon frequency, but it is better described as an "effective attempt frequency" not only because the charge carrier may be coupled to different (and multiple!) phonon modes in the HT and LT phases but also because of the possibility of nonadiabatic processes, which decrease the probability of successful hopping events.[31]

In summary, we can say that the conductivity change upon the charge transfer phase transition in Rb$_x$Mn[Fe(CN)$_6$]$_y$·zH$_2$O is determined mainly by the variation of the preexponential factor. Since the constants involved in σ_0 (i.e., the hopping distance, the phonon frequency, and density of donor–acceptor pairs) change little from one phase to another or from one stoichiometry to another, the value of σ_0 is expected to vary less than an order of magnitude upon the phase transition, which has been confirmed here experimentally. We believe that the comparable activation energy values in the HT and LT phases occur only fortuitously. For example, one may speculate that the shorter distances in the LT phase imply higher force constants. Assuming parabolic potential energy curves, the former will lead to a smaller activation energy due to the proximity of the potential wells, whereas the later will increase the barrier due to the higher curvature of the wells. In certain circumstances, the two effects might thus just cancel each other.

5. Conclusions

We have studied the charge transport in valence-tautomeric Rb$_x$Mn[Fe(CN)$_6$]$_y$·zH$_2$O samples with different stoichiometries. The large bistability domain allowed us to investigate the charge transport in the two valence-tautomeric phases in strictly identical experimental conditions. The frequency-dependent conductivity obeys time–temperature superposition (scaling law) typical to disordered solids. The dc conductivity shows Arrhenius behavior at high temperatures. A dipole relaxation process displaying the same thermal activation energy as the conductivity has also been observed. The overall experimental results were well-reproduced by the equation $\sigma_{dc} = (n_c e^2 a^2/6k_B T)\nu_p$. These characteristics imply a small polaron hopping mechanism of the charge transport, which we assigned, from the sign of the Seebeck coefficient, to the intervalence electron transfer $Mn^{2+}-NC-Fe^{3+} \leftrightarrow Mn^{3+}-NC-Fe^{2+}$.

The valence-tautomeric phase transition is clearly displayed in the thermal hysteresis of the electrical properties. However, at low temperatures, a crossover occurs in the conductivity mechanism from an Arrhenius-type to a variable activation energy behavior, leading to a strange "double-loop" shape of the hysteresis loop. This crossover is typical of small polaron hopping phenomena, and from the investigation of samples that do not display phase transition, we could unambiguously conclude that the two phenomena (the valence-tautomeric phase transition and the crossover in the conductivity mechanism) are independent and occur in the same temperature range in certain samples only by coincidence. On the other hand, the charge transfer phase transition obviously modulates the conductivity, and therefore, the conductivity data reflect both phenomena. Actually, the phase transition does not lead to a modification of the transport and dielectric relaxation mechanisms, but it does modify the conductivity and the relaxation rate. Surprisingly, the activation energy of the conductivity was fairly similar in

the two phases. On the other hand, the charge transfer rate and, as a consequence, the conductivity, as well, are higher in the LT phase. This difference is clearly displayed in the preexponential factor of the hopping frequency, which correlates well, at least qualitatively, with the fact that the HT → LT phase transition involves a strong stiffening of the lattice.

Finally, let us note that it might be possible to determine intervalence electron transfer rates in these compounds using other techniques (muon spin relaxation, Mössbauer spectroscopy, optical absorption, etc.). A comparison of such data with charge transfer rates determined from complex conductivity measurements is a very interesting perspective of the present work.

References and Notes

(1) Robin, M. B.; Day, P. *Adv. Inorg. Chem. Radiochem.* **1967**, *10*, 247.

(2) Dunbar, K.; Heintz, R. A. *Prog. Inorg. Chem.* **1997**, *45*, 283.

(3) Itaya, K.; Uchida, I.; Neff, V. D. *Acc. Chem. Res.* **1986**, *19*, 162.

(4) Verdaguer, M.; Bleuzen, A.; Marvaud, V.; Vaissermann, J.; Seuleiman, M.; Desplanches, C.; Scuiller, A.; Train, C.; Garde, R.; Gelly, G.; Lomenech, C.; Roseman, I.; Veillet, P.; Cartier, C.; Villain, F. *Coord. Chem. Rev.* **1999**, *190−192*, 1023.

(5) Sato, O.; Iyoda, T.; Fujishima, A.; Hashimoto, K. *Science* **1996**, *272*, 704.

(6) Sato, O.; Einaga, Y.; Fujishima, A.; Hashimoto, K. *Inorg. Chem.* **1999**, *38*, 4405.

(7) Sato, O.; Kawakami, T.; Kimura, M.; Hishiya, S.; Kubo, S.; Einaga, Y. *J. Am. Chem. Soc.* **2004**, *126*, 13176.

(8) Tennakone, K.; Dharmaratne, W. G. D. *J. Phys. C: Solid State Phys.* **1983**, *16*, 5633.

(9) Feldman, B. J.; Murray, R. W. *Inorg. Chem.* **1987**, *26*, 1702.

(10) Rosseinsky, D. R.; Tonge, J. S.; Berthelot, J.; Cassidy, J. F. *J. Chem. Soc., Faraday Trans. 1* **1987**, *83*, 231.

(11) Xidis, A.; Neff, V. D. *J. Electrochem. Soc.* **1991**, *138*, 3637.

(12) Moritomo, Y.; Hanawa, M.; Ohishi, Y.; Kato, K.; Takata, M.; Kuriki, A.; Nishibori, E.; Sakata, M.; Ohkoshi, S.; Tokoro, H.; Hashimoto, K. *Phys. Rev. B* **2003**, *68*, 144106.

(13) Tokoro, H.; Matsuda, T.; Hashimoto, K.; Ohkoshi, S. *J. Appl. Phys.* **2005**, *97*, 10M508.

(14) Ohkoshi, S.; Tokoro, H.; Hashimoto, K. *Coord. Chem. Rev.* **2005**, *249*, 1830.

(15) Tokoro, H.; Miyashita, S.; Hashimoto, K.; Ohkoshi, S. *Phys. Rev. B* **2006**, *73*, 172415.

(16) Moritomo, Y.; Kato, K.; Kuriki, A.; Takata, M.; Sakata, M.; Tokoro, H.; Ohkoshi, S.; Hashimoto, K. *J. Phys. Soc. Jpn.* **2002**, *71*, 2078.

(17) Yokoyama, T.; Tokoro, H.; Ohkoshi, S.; Hashimoto, K.; Okamoto, K.; Ohta, T. *Phys. Rev. B* **2002**, *66*, 184111.

(18) Ohkoshi, S.; Matsuda, T.; Tokoro, H.; Hashimoto, K. *Chem. Mater.* **2005**, *17*, 81.

(19) Vertelman, E. J. M.; Maccallini, E.; Gournis, D.; Rudolf, P.; Bakas, T.; Luzon, J.; Broer, R.; Pugzlys, A.; Lummen, T. T. A.; van Loosdrecht, P. H. M.; van Koningsbruggen, P. J. *Chem. Mater.* **2006**, *18*, 1951.

(20) Vertelman, E. J. M.; Lummen, T. T. A.; Meetsma, A.; Bouwkamp, M. W.; Molnar, G.; van Loosdrecht, P. H. M.; van Koningsbruggen, P. J. *Chem. Mater.* **2008**, *20*, 1236.

(21) Dordor, P.; Marquestaut, E.; Villeneuve, G. *Rev. Phys. Appl.* **1980**, *15*, 1607.

(22) Dyre, J. C.; Schroder, T. B. *Rev. Mod. Phys.* **2000**, *72*, 873.

(23) Ohkoshi, S.; Nuida, T.; Matsuda, T.; Tokoro, H.; Hashimoto, K. *J. Mater. Chem.* **2005**, *15*, 3291.

(24) Jonscher, A. K. *Dielectric Relaxation in Solids*, Chelsea Dielectric Press: London, 1983.

(25) Macedo, P. B.; Moynihan, C. T.; Bose, R. *Phys. Chem. Glasses* **1972**, *13*, 171.

(26) Mott, N. F.; Davis, E. A. *Electronic Processes in Non-Crystalline Materials*, Clarendon: Oxford, 1979.

(27) Sayer, M.; Mansingh, A. *Phys. Rev. B* **1972**, *6*, 4629.

(28) Austin, I. G.; Mott, N. F. *Adv. Phys.* **1969**, *18*, 41.

(29) Cobo, S; Fernández, R.; Salmon, L; Molnár, G.; Bousseksou, A *Eur. J. Inorg. Chem.* **2007**, 1549.

(30) Havriliak, S.; Negami, S. *Polymer* **1967**, *8*, 161.

(31) In the nonadiabatic case, the preexponential factor and, thus, the hopping probability, as well, will be further reduced by a factor of $\exp(-\alpha a)$ where α is the reciprocal state localization amplitude (i.e., the tunneling probability).[26]